

1 **Unveiling Amplified Isolation in Climate Networks due**
2 **to Global Warming**

3 Yifan Cheng¹, Panjie Qiao^{1*}, Meiyi Hou², Yuan Chen¹, Wenqi Liu¹ and Yongwen
4 Zhang^{1*}

5 ¹ Data Science Research Center, Faculty of Science, Kunming University of Science and Technology,
6 Kunming 650500, China;

7 ² Department of Atmospheric Sciences, Yunnan University, Kunming, China.

8 *Correspondence to: Yongwen Zhang (zhangyongwen77@gmail.com), and Panjie Qiao
9 (qiaopanjie0720@163.com)

10 **Abstract**

11 Our study utilizes global reanalysis of near-surface daily air temperature data, spanning from 1949 to
12 2019, to construct climate networks. By employing community detection for each year, we reveal the
13 evolving community structure of the climate network within the context of global warming. Our
14 findings indicate significant changes in measures such as the network modularity and the number of
15 communities, over the past 30 years. Notably, the community structure of the climate network
16 undergoes a discernible transition since the early 1980s. We attribute this transition to the substantial
17 increase in isolated nodes since the 1980s, primarily concentrated in equatorial ocean regions.
18 Additionally, we demonstrate that nodes experiencing amplified isolation tend to diminish connectivity
19 with other nodes globally, particularly those within the same oceanic basin, while showing a significant
20 strengthening of connections with the Eurasian and North African continents. We deduce that the
21 mechanism driving amplified isolation in the climate network may be comprehended through the

22 weakening of tropical circulations such as the Hadley cell and the Walker circulation in response to
23 increasing greenhouse gases.

24 **1 Introduction**

25 Since the 20th century, with the continuous increase of greenhouse gas emissions, the global
26 climate system is undergoing warming (IPCC, 2023; Christopher et al., 2012; Hallegatte et al., 2011;
27 Hunt and Watkiss, 2011). Global warming has led to a significant increase in various extreme weather
28 events, encompassing extreme heatwaves, cold spells, heavy precipitation, droughts, and severe
29 hurricanes etc. (Doney et al., 2009; Mondal et al., 2021; Konapala et al., 2020; Mukherjee et al., 2020).
30 In addition, it has a serious impact on global air quality, food production, energy consumption,
31 transportation, water resources, economic and ecosystems, etc. (Thomas et al., 2004; Salehyan and
32 Hendrix, 2014; Nordhaus and William, 2017; Burke et al., 2015). Global warming has triggered
33 significant transformations in atmospheric circulation and ocean circulation patterns, impacting the
34 dynamics of the Earth's climate system (Shepherd, 2014; Vecchi et al., 2007). The rise in global
35 temperatures is a key driver of alterations in atmospheric circulation patterns, especially in the tropical
36 belt, influencing phenomena such as the Hadley Cell, Walker Circulation, and the Madden-Julian
37 oscillation (Lu et al., 2007; Tokinaga et al., 2012; Hu et al., 2021; Chang et al., 2015). The expansion
38 of the tropics and changes in the distribution of sea surface temperatures contribute to shifts in the
39 intensity and frequency of tropical cyclones and the behavior of the El Niño-Southern Oscillation
40 (ENSO) (Emanuel et al., 2005; Kossin et al., 2020; Cai et al., 2021). These modifications in tropical
41 circulations have widespread implications for precipitation patterns, extreme weather events, and
42 regional climate variability. Additionally, the Atlantic Meridional Overturning Circulation (AMOC)
43 may undergo a transition, with potential collapse having severe impacts on the climate in the North

44 Atlantic and European regions (Rahmstorf et al., 2015; Boers, 2021). Previous studies have argued that
45 the global climate experienced a shift in the 1970s (Graham, 1994; Tsonis et al., 2007; Swanson et al.,
46 2009). Understanding these systematic changes is imperative for predicting future climate scenarios
47 (e.g., precipitation, temperature and wind) and formulating effective adaptation and mitigation
48 strategies.

49 Faced with these climatic systematic changes, the adoption of complex network analysis has
50 become increasingly essential in the realm of climate science. The climate system is intricately
51 complex, marked by multivariable and multiscale nonlinear dynamics. Unveiling the internal structure
52 of the climate system necessitates the application of sound research methods. Complex network
53 analysis emerges as a potent tool for investigating the nonlinear dynamics and structural characteristics
54 of complex systems (Newman, 2018; Zou et al., 2019). Over the past several years, complex network
55 methodologies have gained widespread application in the realm of climate science. In the climate
56 network, nodes represent geographical locations where time series data for temperature (or other
57 climate variables) are accessible. Links are established through bivariate similarity measures such as
58 correlation, mutual information, or event synchronization between these time series (Tsonis et al.,
59 2004; Donges et al., 2009; Quiroga et al., 2002). Climate network techniques have proven effective in
60 enhancing our understanding of various climate and weather phenomena, including ENSO,
61 teleconnection patterns of weather, and atmospheric pollution (Tsonis et al., 2008; Yamasaki et al.,
62 2008; Fan et al., 2017; Kittel et al., 2021; Zhou et al., 2015; Boers et al., 2019; Capua et al., 2020;
63 Zhang et al., 2019). Notably, complex network analysis has unveiled the weakening of tropical
64 circulation under global warming (Geng et al., 2021; Fan et al., 2018). Furthermore, these techniques

65 have demonstrated utility in forecasting climate events (Boers et al., 2014; Ludescher et al., 2014;
66 Meng et al., 2018; Ludescher et al., 2021).

67 Complex systems naturally exhibit partitioning into multiple modules or communities, a
68 significant feature of complex networks (Palla et al., 2005). In the context of climate networks, each
69 community serves as a representation of a climate subsystem, shedding light on the interrelationships
70 between different components (Tsonis et al., 2011). Community detection algorithms, rooted in
71 modularity maximization (Newman, 2006; Cherifi et al., 2019), have been pivotal in unveiling
72 structures within climate networks. These algorithms have successfully identified community structures
73 in diverse contexts, including rainfall networks (Agarwal et al., 2018), interaction networks of sea
74 surface temperature observations (Tantet et al., 2014), global climate responses to ENSO phases (Kittel
75 et al., 2021) and the quantification of climate indices. Yet, scant attention has been given to the impact
76 of global warming on the community structure of climate networks, particularly those with small sizes.
77 This research endeavors to employ network analysis and community detection to investigate how
78 global warming is reshaping the structure of the global temperature network. The ultimate goal is to
79 deepen our understanding of climate change and inform strategies for addressing its impacts.

80 Therefore, based on the near-surface temperature structure climate network, this paper studies the
81 impact of global warming on climate network. Employing the Louvain community detection algorithm,
82 it analyzes the evolution of network topology and reveals the underlying factors driving changes in the
83 network structure. The main structure of this paper is as follows: Section 2 and 3 introduce the data and
84 methods; Section 4 shows the results of the evolution of climate network topology; Section 5
85 summarizes the results.

86 2 Data

87 This study utilizes daily air temperature reanalysis data from the National Centers for
88 Environmental Prediction (NCEP) and the National Center for Atmospheric Research (NCAR) at a
89 resolution of $2.5^\circ \times 2.5^\circ$, spanning the near-surface (sig995 level) temperatures from 1949 to 2019
90 (Kalnay et al.,1996). The dataset comprises 10,512 grid points over the global. We select 726 nodes to
91 construct the network and maintain the spatial density homogeneity within the climate network nodes
92 in the sphere as suggested in previous studies (Zhou et al., 2015; Guez et al., 2014). These nodes are
93 strategically spaced to ensure uniform coverage of the Earth in Euclidean space, as depicted in
94 Supplementary Fig. S1(a). The nodes are equally distributed, with distances between any two
95 neighboring nodes approximately 850 km, as illustrated in Supplementary Fig. S1(b).

96 3 Methods

97 3.1 Constructing the climate network

98 Climate networks are constructed based on the near-surface air temperature data for each year
99 from 1949 to 2019, resulting in a total of 71 established climate networks. The time series of a node
100 (denoted as i) undergoes deseasonalization by subtracting the average seasonal cycle and dividing by
101 the standard deviation of the cycle, resulting in the temperature anomaly (denoted as $T_i^y(t)$, where y
102 is the index of year) (Fan et al.,2018). To obtain the link strength between each pair of nodes i and j ,
103 we then calculate the time-lagged cross-correlation function(Fan et al., 2021):

$$104 \quad C_{ij}^y(-\tau) = \frac{\langle T_i^y(t)T_j^y(t-\tau) \rangle - \langle T_i^y(t) \rangle \langle T_j^y(t-\tau) \rangle}{\sqrt{\langle (T_i^y(t) - \langle T_i^y(t) \rangle)^2 \rangle} \cdot \sqrt{\langle (T_j^y(t-\tau) - \langle T_j^y(t-\tau) \rangle)^2 \rangle}}, \quad (1)$$

$$105 \quad C_{ij}^y(\tau) = \frac{\langle T_i^y(t-\tau)T_j^y(t) \rangle - \langle T_i^y(t-\tau) \rangle \langle T_j^y(t) \rangle}{\sqrt{\langle (T_i^y(t-\tau) - \langle T_i^y(t-\tau) \rangle)^2 \rangle} \cdot \sqrt{\langle (T_j^y(t) - \langle T_j^y(t) \rangle)^2 \rangle}}, \quad (2)$$

106 where $\langle \rangle$ denotes the mean value, based on which $\langle f(a) \rangle = \frac{1}{365} \sum_{t=1}^{365} f(t - a)$; t represents time and
 107 the time lag is denoted as $\tau \in [0, 200]$ days.

108 Therefore, the link strength between each pair of nodes in the network is denoted as follows:

$$109 \quad W_{ij}^y = \frac{\max(C_{ij}^y(\tau)) - \text{mean}(C_{ij}^y(\tau))}{\text{std}(C_{ij}^y(\tau))}, \quad (3)$$

110 in this context, “*max*”, “*mean*” and “*std*” denote the maximum value, mean, and standard
 111 deviation of the cross-correlation over all time lags from -200 to 200 days between nodes i and j .
 112 Strong autocorrelation can inflate the significance of cross-correlation. In contrast, the link strength
 113 W_{ij}^y is more effective in mitigating the effects of autocorrelation, offering a more reasonable reflection
 114 of the relationship between two nodes (Guez et al., 2014). This approach has proven valuable in
 115 predicting climate phenomena (Ludescher et al., 2021). To select meaningful links in the network and
 116 eliminate false associations. A threshold of $\theta = 3.5$ (corresponding to a p-value of 0.03 (Palus et al.,
 117 2011) signifying that 97% of the values in the shuffled data fall below this threshold in Supplementary
 118 Fig. S2) is applied to obtain an adjacency matrix \mathbf{A} (when $W_{ij}^y \geq \theta$, the element $A_{ij} = 1$, otherwise,
 119 the element $A_{ij} = 0$).

120 3.2 Community Detection

121 Subsequently, the obtained sequence of climate networks underwent community detection using
 122 the Louvain community detection algorithm. The key steps of this method involve traversing each node
 123 in the network and attempting to relocate it to a neighboring node in a different community to optimize
 124 the modularity Q . If moving a node to another community increases the modularity, the move is
 125 executed; otherwise, it remains unchanged. In other words, the process assesses whether the increment
 126 in modularity ΔQ resulting from the move is positive, and this procedure is repeated until no further
 127 node movements are possible. Here is the formula for calculating modularity (Blondel et al., 2008):

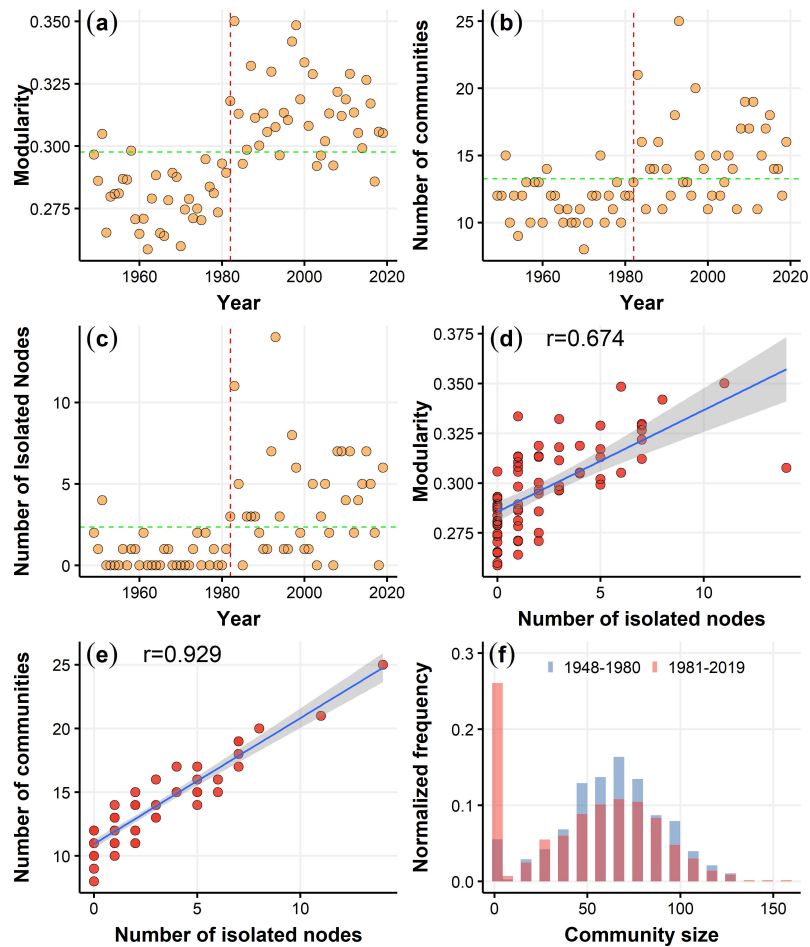
$$128 \quad Q = \frac{1}{2m} \sum_{i,j} [A_{ij} - \frac{k_i k_j}{2m}] \delta(c_i, c_j), \quad (4)$$

129 where $k_i = \sum_j A_{ij}$ and $k_j = \sum_i A_{ij}$ ($i \neq j$) are the number of links connected to vertex (node) i and
130 j , c_i represents the community to which node i belongs, $\delta(\mu, \nu)$ equals 1 if $\mu = \nu$, otherwise 0, and
131 $m = \frac{1}{2} \sum_{ij} A_{ij}$. Modularity has become a metric for assessing the quality of community divisions, with
132 high modularity indicating strong internal connections within a community and weaker connections
133 with other communities.

134 **4 Results**

135 In order to investigate the evolution of the network's topology in the context of global warming,
136 we construct the network for each year from 1949 to 2019 and apply community detection to the
137 network. In Fig. 1(a), we show that the network modularity for the early years (1949-1981) is largely
138 below the average level. While in the recent years (1982-2019), the network modularity remain
139 consistently above the average level. There is a significant transition in the modularity around 1982.
140 Supplementary Fig. S3 illustrates the modularity values obtained by four distinct algorithms, as
141 outlined in Ref (Kittel et al., 2021). The results highlight the robustness of the modularity transition
142 around 1982 across different algorithms. Notably, the Louvain algorithm produces the highest
143 modularity values, indicating its superior effectiveness in identifying community structures. The
144 number of communities and modularity exhibit similar evolutionary patterns as shown in Fig. 1(b).
145 Although the trend in the change of the number of communities is not as pronounced as the trend in
146 network modularity, it is still evident that the number of communities was mostly below the average
147 level in the first 33 years, while in the recent 38 years, the majority of community numbers are above
148 the average level (as shown in Fig. 1(b)). Fig. 1(c) also shows the escalating count of isolated nodes
149 since 1982. The isolated node is identified by the Louvain algorithm with a community size of 1
150 (equivalent to a degree of zero, $k_i = 0$). The observed systematic change in community structure since

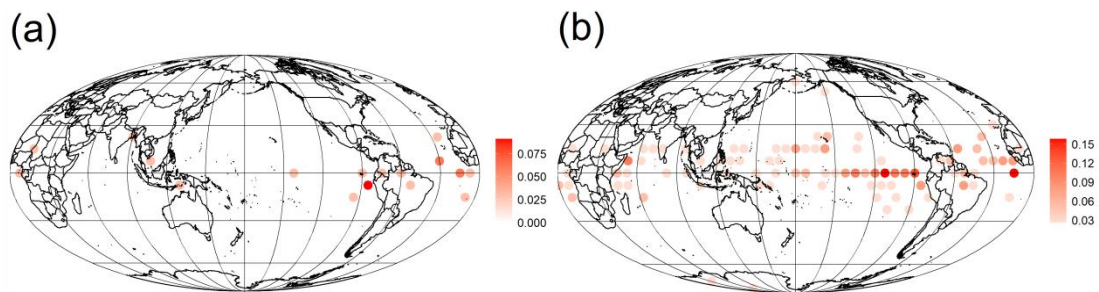
151 the early 1980s could be linked to the reported climate shift, as indicated by Refs (Graham, 1994;
 152 Tsonis et al., 2007; Swanson, 2009) utilizing both reanalysis data and climate simulations. The
 153 substantial increase in greenhouse gas emissions has contributed to a shift in the mean climate state
 154 since the 1980s in the tropical belt (Cai et al., 2021). This shift is further evident in the altered
 155 properties of El Niño since the early 1980s (Gan et al., 2023).



156
 157 **Figure 1.** Temporal evolution of (a) network modularity, (b) the number of communities and (c) the number
 158 of isolated nodes from 1949 to 2019, illustrated by the green dashed line denoting the average level, and the
 159 red dashed line represents the transition around 1982. Scatter plot of (d) the network modularity, (e) the
 160 number of communities versus the number of isolated nodes during the period 1949-2019. (f) The
 161 normalized frequencies of community size for 1949-1981 and 1982-2019 respectively (normalized by the
 162 total number of communities for each period), where the first bar represents the normalized frequency of
 163 the community with a node.

164 Since 1982, the number of communities has been on the rise. This trend appears to be closely

165 linked to the increasing count of isolated nodes. We observe the relationship between modularity and
166 the number of isolated nodes and find a strong positive correlation with a correlation coefficient of
167 0.674 (as shown in Fig. 1(d)). The high correlation with network modularity indicates that the trend in
168 the number of isolated nodes is consistent with changes in the network's topological structure.
169 Furthermore, from Fig. 1(e), we observe that the correlation between the number of isolated nodes and
170 the number of communities reaches 0.929. The high correlation with the number of communities
171 suggests that the overall increase in the number of communities is driven by the increase in isolated
172 nodes. To further strengthen the verification of whether the changes in the number of communities and
173 network modularity since 1982 are related to the number of isolated nodes. We examine the normalized
174 frequency of community sizes in 1949-1981 and 1982-2019 (as shown in Fig. 1(f)). There are two
175 peaks for the isolated node and the community with size around 60 for both 1949-1981 and 1982-2019.
176 In 1949-1981, the proportion of isolated nodes in the overall community is not prominent. However, in
177 1982-2019, the proportion of isolated nodes has dramatically increased and has become the largest
178 component in the community distribution. Therefore, the transition in modularity and the number of
179 communities since 1982 can be attributed to the substantial increase in the number of isolated nodes.
180



181

182 **Figure 2. Occurrence probability maps of isolated nodes for (a) 1949-1981, and (b) 1982-2019.**

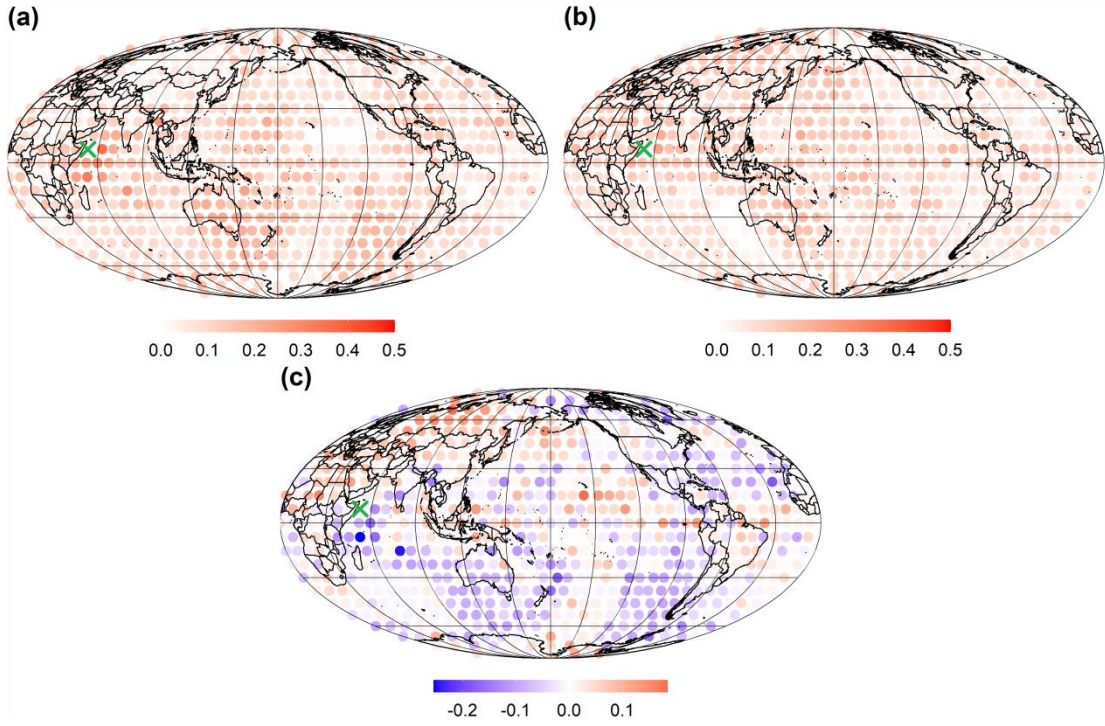
183 Next, we will further study the relationship between changes in climate network structure and
184 isolated nodes. The occurrence probability maps of isolated nodes for 1949-1981 and 1982-2019 are
185 shown in Fig. 2. From 1949 to 1981, few isolated nodes are mainly distributed in the Equatorial East
186 Pacific and Equatorial Atlantic oceans, with a low occurrence probability. However, from 1982 to 2019,
187 the isolated nodes with higher occurrence probabilities can appear almost everywhere in the equatorial

188 regions such that the total number of communities increase. The occurrence probability of isolated
189 nodes in the last 38 years is not only higher than the first 33 years but also covers a larger area than the
190 first 33 years. Hence, isolated nodes in the equatorial region have been systematically increasing since
191 the early 1980s, resulting in changes to the climate network structure. To establish robustness, we
192 conduct the analysis using different community detection algorithms, the maximum time lag of 365
193 days, the shuffled nodes and a 6-month shift for the time window. The obtained results are consistent,
194 as illustrated in Supplementary Figs. S3-S12.

195 To gain a deeper understanding and verify how the isolation in climate networks is amplified in
196 the Equatorial regions, we select three nodes with the highest frequency of isolation in three regions:
197 the Indian Ocean, the Pacific Ocean, and the Atlantic Ocean, respectively. We study the relationships
198 between the three nodes and other nodes across the climate network structure. Specifically, we
199 calculate the probability of the selected node and each of other 725 nodes belonging to the same
200 community for time periods 1949-1981 and 1982-2019, and compute the difference the two time
201 periods. This probability can reflect which important region responds to the amplified isolation of the
202 selected node.

203 In Fig. 3(a), for 1949-1981, the selected Indian Ocean node exhibits high probability with
204 surrounding nodes belonging to the same community. However, for the 1982-2019 in Fig. 3(b), this
205 probability is weakened, particularly in their association with the oceanic regions. the difference of the
206 probability between 1982-2019 and 1949-1981 is shown in Fig. 3(c). Blue (red) points in Fig. 3(c)
207 represent the decreased (increased) probability with time. In general, most areas have decreased
208 probability. Still, some areas i.e., the Eurasian and North Africa continent have increased probability to
209 connect to the selected Indian Ocean node.

210 Since the 1980s, the probabilities of the nodes in the Pacific and the equatorial Pacific region
211 belonging to the same community are noticeably diminished (as shown in Fig. 4). Examining the
212 probability map of the selected Atlantic Ocean node and other global nodes belonging to the same
213 community in Fig. 5, it is observed a similar behavior. The selected three high-frequency isolated
214 nodes are surrounded by relatively strong connectivity regions during the first 33 years. However, these
215 regions experience varying degrees of weakening in connectivity during the subsequent 38 years. It is
216 worth noting that since the 1980s, the connectivity between high-frequency isolated nodes in the Indian
217 Ocean, Atlantic Ocean, and Pacific Ocean with global oceanic regions is diminishing, especially the
218 strength of their connections with their respective oceanic regions significantly decreasing. However,
219 the association with the Eurasian and North Africa continent is strengthening. Previous studies have
220 suggested the weakening of tropical circulations such as the Hadley cell and the Walker circulation, in
221 response to increasing greenhouse gases (Lu et al., 2007; Tokinaga et al., 2012; Cai et al., 2021). This
222 weakening may contribute to the amplified isolation of nodes in tropical oceans. Additionally, the
223 weakened tropical circulation could potentially trigger extreme climate phenomena, such as the
224 intensification of El Niño, with more pronounced teleconnection impacts on distant regions (Fan et al.,
225 2017; Hu et al., 2021). This could, in turn, strengthen the linkage between equatorial regions and
226 continents in climate networks.

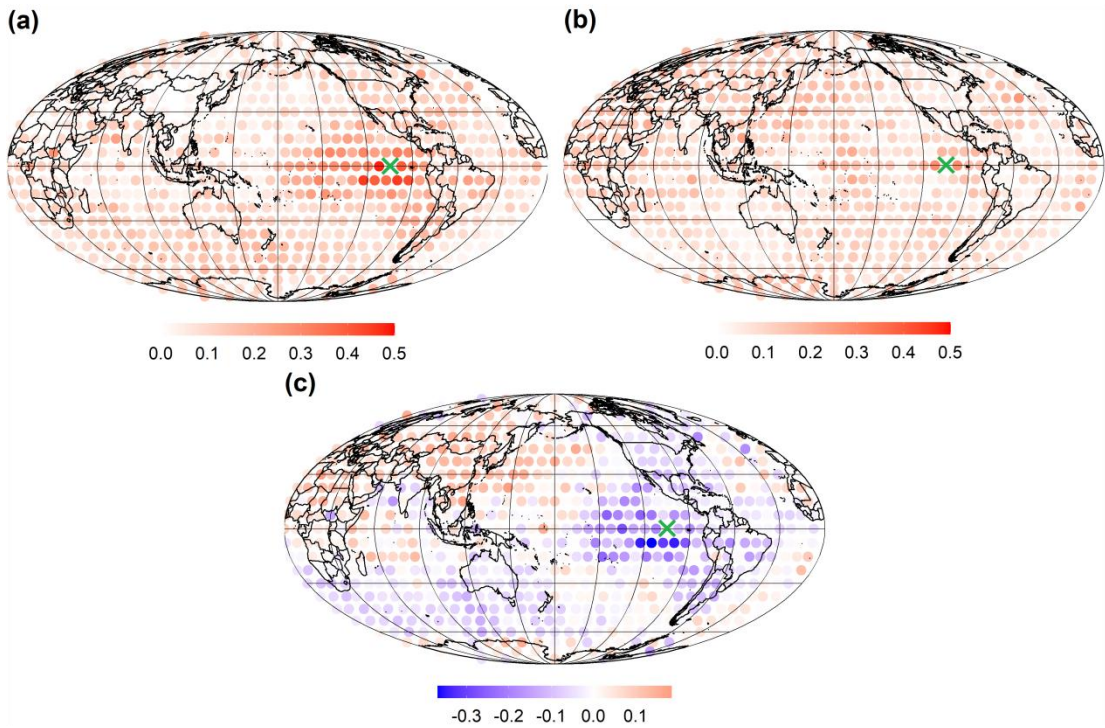


227

228 **Figure 3. Probability maps of the Indian Ocean node and other global nodes belonging to the same**

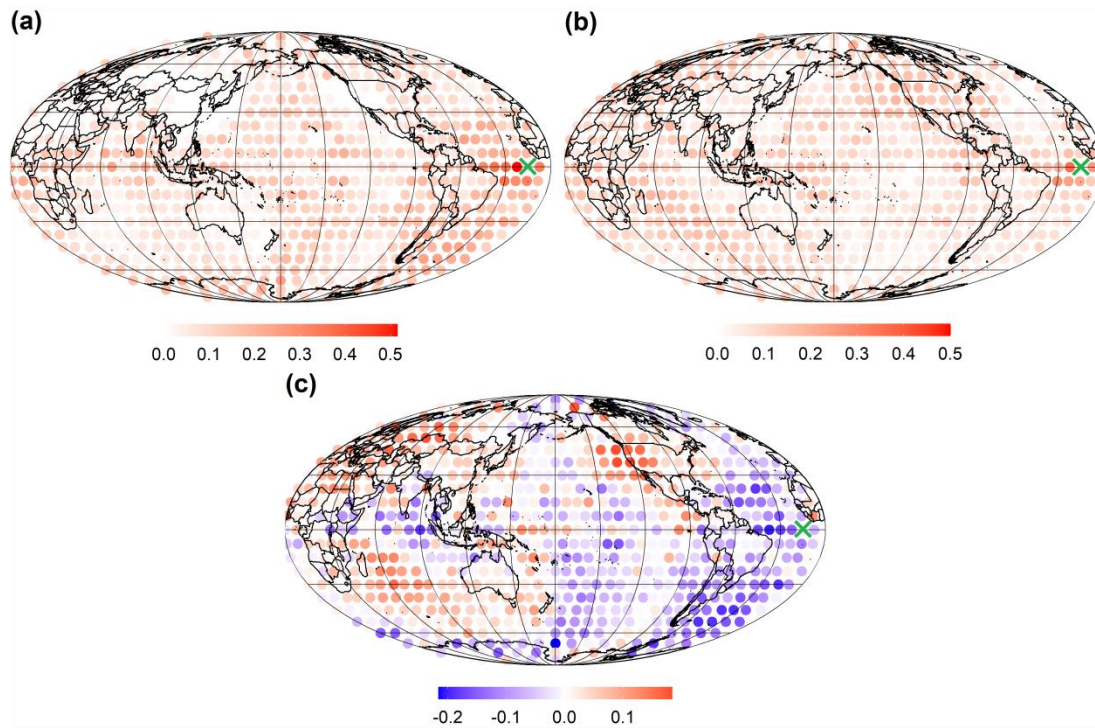
229 **community for (a) 1949-1981, (b) 1982-2019, and (c) the difference of the probability between 1982-2019 and**

230 **1949-1981. The symbol of cyan cross represents the selected Indian Ocean node.**



231

232 Figure 4. Probability maps of the Eastern Pacific Ocean node and other global nodes belonging to the same
233 community for (a) 1949-1981, (b) 1982-2019, and (c) the difference of the probability between 1982-2019 and
234 1949-1981. The symbol of cyan cross represents the selected Eastern Pacific Ocean node.



235
236 Figure 5. Probability maps of the Atlantic Ocean node and other global nodes belonging to the same
237 community for (a) 1949-1981, (b) 1982-2019, and (c) the difference of the probability between 1982-2019 and
238 1949-1981. The symbol of cyan cross represents the selected Atlantic Ocean node.

239 5 Conclusions

240 In this investigation, we constructed a climate network using near-surface air temperature data
241 spanning from 1949 to 2019. Our aim is to examine the evolution of climate network topology within
242 the context of global warming. To explore how global warming affects the structure of the global
243 climate network, we applied the Louvain community detection algorithm.

244 Notably, we observed that the network modularity between 1949 and 1981 remained below the
245 overall average, whereas between 1982 and 2019, it exceeded the overall average. Concurrently, the

246 trend in the number of communities from 1949 to 2019 followed a similar pattern to that of modularity.
247 Furthermore, the correlation coefficient between modularity and the number of isolated nodes was
248 found to be 0.674. Additionally, the correlation between the number of isolated nodes and the number
249 of communities reached 0.929, both of which demonstrated statistical significance. Furthermore, we
250 noted a substantial increase in the number of isolated nodes since 1982. Hence, the shift in modularity
251 and the number of communities since 1982 are significantly associated with the notable surge in the
252 number of isolated nodes. This systematic shift in community structure since the early 1980s could be
253 related to the climate shift and the change of mean state associated with the altered properties of El
254 Niño since the early 1980s (Graham, 1994; Tsonis et al., 2007; Swanson, 2009; Cai et al., 2021; Gan et
255 al., 2023).

256 Between 1949 and 1981, isolated nodes were sporadic and dispersed, mainly concentrated in the
257 equatorial Pacific and equatorial Atlantic regions. However, from 1982 to 2019, isolated nodes were
258 pervasive across the entire equatorial oceanic region. We further examined the relationship between
259 temperature network structure and isolated nodes in the context of global warming. By selecting key
260 nodes with the highest frequency of isolation in the equatorial Pacific, equatorial Atlantic, and
261 equatorial Indian Ocean regions, we investigated their likelihood of belonging to the same community
262 as other nodes during 1949-1981 and 1982-2019. Our findings suggested that the connectivity of highly
263 isolated nodes along the equator is decreasing, potentially associated with the weakening of tropical
264 circulations such as the Hadley cell and the Walker circulation in response to increasing greenhouse
265 gases. This is particularly notable concerning their associations with neighboring regions within the
266 same oceanic basin. Simultaneously, their connections with certain continents have significantly
267 strengthened.

268

269 **Acknowledgements**

270 We thank the financial support by the National Natural Science Foundation of China (Grant No.
271 12305044 and 12371460), and the National Key Research and Development Program of China
272 (Grant No. 2023YFE0109000).

273

274 **Data Availability**

275 The data that support the findings of this study are publicly available online: NCEP/NCAR reanalysis
276 near-surface (sig995 level) daily air temperature data,
277 <https://psl.noaa.gov/data/gridded/data.ncep.reanalysis.html>, accessed on 14 September 2022.

278

279 **Author Contributions**

280 Yi.C.: Investigation, Visualization, Analysis, Writing-Original draft, Reviewing, Editing. P.Q. :
281 Methodology, Writing, Reviewing, Editing. M.H.: Methodology, Writing, Reviewing, Editing. Yuan.C.:
282 Methodology, Writing, Reviewing, Editing. W.L.: Methodology, Writing, Reviewing, Editing. Y.Z.:
283 Investigation, Conceptualization, Analysis, Methodology, Writing, Reviewing, Editing, Supervision.

284

285 **Competing interests**

286 The contact author has declared that none of the authors has any competing interests.

287

288 **Disclaimer**

289 Publisher's note: Copernicus Publications remains neutral with regard to jurisdictional claims in

290 published maps and institutional affiliations.

291

292 **Financial support**

293 This study was supported by the National Natural Science Foundation of China (No. 12305044 and No.
294 12371460) and the National Key Research and Development Program of China (Grant No.
295 2023YFE0109000).

296

297 **References**

298 Agarwal, A., Marwan, N., Maheswaran, R., Merz, B., and Kurths, J.: Quantifying the roles of single
299 stations within homogeneous regions using complex network analysis, *J. Hydrol.*, 563:802-10,
300 <https://doi.org/10.1016/j.jhydrol.2018.06.050>, 2018.

301 B.F. Christopher, V. Barros, T. F. Stocker and Q. Dahe: Managing the risks of extreme events and
302 disasters to advance climate change adaptation: special report of the intergovernmental panel on
303 climate change, CUP: Cambridge, UK , <https://doi.org/10.1017/CBO9781139177245>, 2012.

304 Blondel, V. D., Guillaume, J. L., Lambiotte, R., and Lefebvre, E.: Fast unfolding of communities in
305 large networks, *J. Stat. Mech.*, P10008, <https://doi.org/10.1088/1742-5468/2008/10/P10008>, 2008.

306 Boers, N., Bookhagen, B., Barbosa, H. M., Marwan, N., Kurths, J., and Marengo, J. A.: Prediction of
307 extreme floods in the eastern Central Andes based on a complex networks approach, *Nat. Commun.*, 5,
308 5199, <https://doi.org/10.1038/ncomms6199>, 2014.

309 Boers, N., Goswami, B., Rheinwalt, A., Bookhagen, B., Hoskins, B., and Kurths, J.: Complex networks
310 reveal global pattern of extreme-rainfall teleconnections, *Nature*, 566, 373-377,
311 <https://doi.org/10.1038/s41586-018-0872-x>, 2019.

312 Boers, N.: Observation-based early-warning signals for a collapse of the Atlantic Meridional
313 Overturning Circulation, *Nat. Clim. Change.*, 11, 680-688,
314 <https://doi.org/10.1038/s41558-021-01097-4>, 2021.

315 Burke, M., Hsiang, S. M., and Miguel, E.: Global non-linear effect of temperature on economic

316 production, *Nature*, 527, 235-239, <https://doi.org/10.1038/nature15725>, 2015.

317 Cai, W., Santoso, A., Collins, M. et al.: Changing El Niño – Southern Oscillation in a warming climate,
318 *Nat Rev Earth Environ*, 2, 628 – 644, <https://doi.org/10.1038/s43017-021-00199-z>, 2021.

319 CCherifi, H., Palla, G., Szymanski, B. K., and Lu, X.: On community structure in complex networks:
320 challenges and opportunities, *Appl. Netw. Sci.*, 4, 117, <https://doi.org/10.1007/s41109-019-0238-9>,
321 2019.

322 Chang, C. W. J., Tseng, W. L., Hsu, H. H., Keenlyside, N., and Tsuang, B. J.: The Madden-Julian
323 Oscillation in a warmer world, *Geophys. Res. Lett.*, 42, 6034-6042,
324 <https://doi.org/10.1002/2015GL065095>, 2015.

325 Di Capua, G., Kretschmer, M., Donner, R. V., Van Den Hurk, B., Vellore, R., Krishnan, R., and
326 Coumou, D.: Tropical and mid-latitude teleconnections interacting with the Indian summer monsoon
327 rainfall: a theory-guided causal effect network approach, *Earth Syst. Dynam.*, 11, 17-34,
328 <https://doi.org/10.5194/esd-11-17-2020>, 2020.

329 Doney, S. C., Fabry, V. J., Feely, R. A., and Kleypas, J. A.: Ocean Acidification: The other CO₂
330 problem, *Annu. Rev. Mar. Sci.*, 1, 169-192, <https://doi.org/10.1146/annurev.marine.010908.163834>,
331 2009.

332 Donges, J. F., Zou, Y., Marwan, N., and Kurths, J.: Complex networks in climate dynamics, *Eur. Phys.*
333 *J. Spec. Top.*, 174, 157 – 179, <https://doi.org/10.1140/epjst/e2009-01098-2>, 2009.

334 Emanuel, K.: Increasing destructiveness of tropical cyclones over the past 30 years, *Nature* 436,
335 686-688, <https://doi.org/10.1038/nature03906>, 2005.

336 Fan, J., Meng, J., Ashkenazy, Y., Havlin, S., and Schellnhuber, H. J.: Network analysis reveals
337 strongly localized impacts of El Niño, *Proc. Natl. Acad. Sci. U.S.A.*, 114, 7543-7548,
338 <https://doi.org/10.1073/pnas.1701214114>, 2017.

339 Fan, J., Meng, J., Ashkenazy, Y., Havlin, S., and Schellnhuber, H. J.: Climate network percolation
340 reveals the expansion and weakening of the tropical component under global warming, *Proc. Natl.*
341 *Acad. Sci. U.S.A.*, 115, E12128-E12134, <https://doi.org/10.1073/pnas.1811068115>, 2018.

342 Fan, J., Meng, J., Ludescher, J., Li, Z., Surovyatkina, E., Chen, X. et al.: Network-based approach and
343 climate change benefits for forecasting the amount of Indian monsoon rainfall, *Am. Meteorol. Soc.*,
344 35(3), 1009-1020, <https://doi.org/10.1175/JCLI-D-21-0063.1>, 2021.

345 Gan, R., Liu, Q., Huang, G., Hu, K., and Li, X.: Greenhouse warming and internal variability increase

346 extreme and central Pacific El Niño frequency since 1980, *Nat. Commun.*, 14, 394,
347 <https://doi.org/10.1038/s41467-023-36053-7>, 2023.

348 Geng, Z., Zhang, Y., Lu, B., Fan, J., Zhao, Z., and Chen, X.: Network-Synchronization Analysis
349 Reveals the Weakening Tropical Circulations, *Geophys. Res. Lett.*, 48, e2021GL093582,
350 <https://doi.org/10.1029/2021GL093582>, 2021.

351 Graham, N.E.: Decadal-scale climate variability in the tropical and North Pacific during the 1970s and
352 1980s: observations and model results, *Clim. Dyn.*, 10, 135-162, <https://doi.org/10.1007/BF00210626>,
353 1994.

354 Guez, O. C., Gozolchiani, A. and Havlin, S.: Influence of autocorrelation on the topology of the
355 climate network, *Phys. Rev. E*, 90(6), 062814, <https://doi.org/10.1103/PhysRevE.90.062814>, 2014.

356 Hallegatte, S., Przulski, V., and Vogt-Schilb, A.: Building world narratives for climate change impact,
357 adaptation and vulnerability analyses, *Nat. Clim. Change*, 1, 151-155, [https://doi.org/10.1038/](https://doi.org/10.1038/nclimate1135)
358 [nclimate1135](https://doi.org/10.1038/nclimate1135), 2011.

359 Hu K., Huang, G., Huang, P. et al.: Intensification of El Niño-induced atmospheric anomalies under
360 greenhouse warming, *Nat. Geosci.*, 14, 377-382, <https://doi.org/10.1038/s41561-021-00730-3>, 2021.

361 Hunt, A., and Watkiss, P.: Climate change impacts and adaptation in cities: a review of the literature,
362 *Clim. Change*, 104, 13 – 49, <https://doi.org/10.1007/s10584-010-9975-6>, 2011.

363 Intergovernmental Panel on Climate Change (IPCC). Climate Change 2022-Impacts, Adaptation and
364 Vulnerability: Working Group II Contribution to the Sixth Assessment Report of the Intergovernmental
365 Panel on Climate Change, CUP, <https://doi.org/10.1017/9781009325844>, 2023.

366 Kalnay, E., Kanamitsu, M.R., Kistler, W., Collins, D., Deaven, L., Gandin, M., Iredell, S., Saha, G.,
367 White, J., Woollen et al.: The Ncep/Ncar 40-Year reanalysis project, *Bull. Am. Meteorol. Soc.*, 77,
368 437-472, <http://.doi.org/10.1175/1520-0477>, 1996.

369 Kittel, T., Ciemer, C., Lotfi, N., Peron, T., Rodrigues, F., Kurths, J., and Donner, R. V.: Evolving
370 climate network perspectives on global surface air temperature effects of ENSO and strong volcanic
371 eruptions, *Eur. Phys. J. Spec. Top.*, 230, 3075-3100 , <https://doi.org/10.1140/epjs/s11734-021-00269-9>,
372 2021.

373 Konapala, G., Mishra, A. K., Wada, Y., and Mann, M. E.: Climate change will affect global water
374 availability through compounding changes in seasonal precipitation and evaporation, *Nat Commun*, 11,
375 3044 , <https://doi.org/10.1038/s41467-020-16757-w>, 2020.

376 Kossin, J. P., Knapp, K. R., Olander, T. L., and Velden, C. S.: Global increase in major tropical
377 cyclone exceedance probability over the past four decades, *Proc. Natl. Acad. Sci.*, 117(22):
378 11975-11980, <https://doi.org/10.1073/pnas.1920849117>, 2020.

379 Lu, J., Vecchi, G. A., and Reichler, T. . Reichler: Expansion of the Hadley cell under global warming,
380 *Geophys. Res. Lett.*, 34, L06805, <https://doi.org/10.1029/2006GL028443>, 2007.

381 Ludescher, J., Gozolchiani, A., Bogachev, M. I., Bunde, A., Havlin, S., and Schellnhuber, H. J.: Very
382 early warning of next El Niño, *Proc. Natl. Acad. Sci. U.S.A.*, 111, 2064-2066,
383 <https://doi.org/10.1073/pnas.1323058111>, 2014.

384 Ludescher, J., Martin, M., Boers, N., Bunde, A., Ciemer, C., Fan, J., et al.: Network-based forecasting
385 of climate phenomena, *Proc. Natl. Acad. Sci. U.S.A.*, 118, e1922872118,
386 <https://doi.org/10.1073/pnas.1922872118>, 2021(a).

387 Meng, J., Fan, J., Ashkenazy, Y., Bunde, A., and Havlin, S.: Forecasting the magnitude and onset of El
388 Niño based on climate network, *New J. Phys.*, 20, 043036, <https://doi.org/10.1088/1367-2630/aabb25>,
389 2018.

390 Mondal, S., and Mishra, A. K.: Complex networks reveal heatwave patterns and propagations over the
391 USA, *Geophys. Res. Lett.*, 48, e2020GL090411 , <https://doi.org/10.1029/2020GL090411>, 2021.

392 Mukherjee, S., and Mishra, A. K.: Increase in compound drought and heatwaves in a Warming World,
393 *Geophys. Res. Lett.*, 48(1), e2020GL090617, <https://doi.org/10.1029/2020GL090617>, 2020.

394 Newman, M. E., and Mark.: *Networks*, OUP, 2018.

395 Newman, M. E.: Modularity and community structure in networks, *Proc. Natl. Acad. Sci.*, 103,
396 8577-8582, <https://doi.org/10.1073/pnas.0601602103>, 2006.

397 Nordhaus, W. D.: Revisiting the social cost of carbon, *Proc Natl Acad Sci U.S.A.*, 114(7), 1518,
398 <https://doi.org/10.1073/pnas.1609244114>, 2017.

399 Palla, G., Derényi, I., Farkas, I., and Vicsek, T.: Uncovering the overlapping community structure of
400 complex networks in nature and society, *Nature*, 435, 814-818, <https://doi.org/10.1038/nature03607>,
401 2005.

402 Paluš, M., and Novotná, D.: Northern Hemisphere patterns of phase coherence between
403 solar/geomagnetic activity and NCEP/NCAR and ERA40 near-surface air temperature in period 7-8
404 years oscillatory modes, *Nonlin. Processes Geophys.*, 18, 251-260,
405 <https://doi.org/10.5194/npg-18-251-2011>, 2011.

406 Quiroga, R. Q., Kreuz, T., and Grassberger, P.: Event synchronization: A simple and fast method to
407 measure synchronicity and time delay patterns, *Phys. Rev. E*, 66, 041904,
408 <https://doi.org/10.1103/PhysRevE.66.041904>, 2002.

409 Rahmstorf, S., Box, J. E., Feulner, G., Mann, M. E., Robinson, A., Rutherford, S., and Schaffernicht, E.
410 J.: Exceptional twentieth-century slowdown in Atlantic Ocean overturning circulation, *Nat. Clim.*
411 *Change*, 5, 475-480, <https://doi.org/10.1038/nclimate2554>, 2015.

412 Salehyan, I., and Hendrix, C. S.: Climate shocks and political violence, *Glob. Environ. Change*, 28,
413 134-145, <https://doi.org/10.1016/j.gloenvcha.2014.07.007>, 2014.

414 Shepherd, T. G.: Atmospheric circulation as a source of uncertainty in climate change projections, *Nat.*
415 *Geosci.* 7, 703-708 , <https://doi.org/10.1038/ngeo2253>, 2014.

416 Swanson, K. L., and Tsonis, A. A.: Has the climate recently shifted? *Geophys. Res. Lett.*, 36, L06711,
417 <https://doi.org/10.1029/2008GL037022>, 2009.

418 Tantet, A., and Dijkstra, H. A.: An interaction network perspective on the relation between patterns of
419 sea surface temperature variability and global mean surface temperature, *Earth Syst. Dynam.*, 5, 1-14,
420 <https://doi.org/10.5194/esd-5-1-2014>, 2014.

421 Thomas, C. D., Cameron, A., Green, R. E., Bakkenes, M., Beaumont, L. J., and Collingham, Y. C. et
422 al.: Extinction risk from climate change, *Nature*, 427, 145-148 , <https://doi.org/10.1038/nature02121>,
423 2004.

424 Tokinaga, H., Xie, S. P., Deser, C., Kosaka, Y., and Okumura, Y. M.: Slowdown of the Walker
425 circulation driven by tropical Indo-Pacific warming, *Nature*, 491, 439-443,
426 <https://doi.org/10.1038/nature11576>, 2012.

427 Tsonis, A. A., and Roebber, P. J.: The architecture of the climate network, *Physica A*, 333: 497-504.
428 <https://doi.org/10.1016/j.physa.2003.10.045>, 2004.

429 Tsonis, A. A., and Swanson, K. L.: Topology and Predictability of El Niño and La Niña Networks,
430 *Phys. Rev. Lett.*, 100, 228502, <https://doi.org/10.1103/PhysRevLett.100.228502>, 2008.

431 Tsonis, A. A., Swanson, K., and Kravtsov, S.: A new dynamical mechanism for major climate shifts,
432 *Geophys. Res. Lett.*, 34, L13705, <https://doi.org/10.1029/2007GL030288>, 2007.

433 Tsonis, A. A., Wang, G., Swanson, K. L., Rodrigues, F. A., and Costa, L. D. F.: Community structure
434 and dynamics in climate networks, *Clim. Dyn.*, 37, 933-940,
435 <https://doi.org/10.1007/s00382-010-0874-3>, 2011.

436 Vecchi, G. A., and Soden, B. J.: Global warming and the weakening of the tropical circulation, J.
437 Climate 20(17) : 4316-4340, <https://doi.org/10.1175/JCLI4258.1>, 2007.

438 Yamasaki, K., Gozolchiani, A., and Havlin, S.: Climate networks around the globe are significantly
439 affected by El Niño, Phys. Rev. Lett., 100, 228501, <https://doi.org/10.1103/PhysRevLett.100.228501>,
440 2008.

441 Zhang, Y., Fan, J., Chen, X., Ashkenazy, Y., and Havlin, S.: Significant impact of Rossby waves on air
442 pollution detected by network analysis, Geophys. Res. Lett., 46, 12476 – 12485,
443 <https://doi.org/10.1029/2019GL084649>, 2019.

444 Zhou, D., Gozolchiani, A., Ashkenazy, Y., and Havlin, S.: Teleconnection paths via climate network
445 direct link detection, Phys. Rev. Lett. 115, 268501, <https://doi.org/10.1103/PhysRevLett.115.268501>,
446 2015.

447 Zou, Y., Donner, R. V., Marwan, N., Donges, J. F., and Kurths, J.: Complex network approaches to
448 nonlinear time series analysis, Phys. Rep., 787, 1-97.<https://doi.org/10.1016/j.physrep.2018.10.005>,
449 2019.